European Journal of Radiology Open 11 (2023) 100519

Contents lists available at ScienceDirect

European Journal of Radiology Open

journal homepage: www.elsevier.com/locate/ejro

Original Article

Fat fraction and R2 * values of various liver masses: Initial experience with 6-point Dixon method on a 3T MRI system

Taichi Kitagawa [a], Kazuto Kozaka [a,*], Takashi Matsubara [a], Tetsuya Wakayama [b], Atsushi Takamatsu [a], Tomohiro Kobayashi [a], Kenichiro Okumura [a], Kotaro Yoshida [a], Norihide Yoneda [a], Azusa Kitao [a], Satoshi Kobayashi [a], Toshifumi Gabata [a], Osamu Matsui [a], Jay P. Heiken [c]

[a] Department of Radiology, Kanazawa University Graduate School of Medical Sciences, 13-1, Takara-machi, Kanazawa, Ishikawa 920-8641, Japan
[b] Applied Science Laboratory Japan and Vascular MR, MR Clinical Solutions and Research Collaborations, GE HealthCare, 4-7-127, Asahigaoka, Hino, Tokyo 191-8503, Japan
[c] Department of Radiology, Mayo Clinic College of Medicine, Mayo Clinic, 200, First Street SW, Rochester, MN 55905, USA

HIGHLIGHTS

- High concordance between readers in 6-point Dixon method on 3 T MRI in liver masses.
- Study found discrepancies between readers in some cases due to small or imperceptible masses.
- 6-point Dixon method suitable for liver mass characterization; might yield useful values.

ARTICLE INFO

Keywords:
Liver neoplasms
Chemical shift imaging
Chemotherapy
Image enhancement
Lipid droplets

ABSTRACT

Purpose: To assess the feasibility of the 6-point Dixon method for evaluating liver masses. We also report our initial experience with the quantitative values in various liver masses on a 3T system.

Materials and methods: Of 251 consecutive patients for whom 6-point Dixon was employed in abdominal magnetic resonance imaging scans between October 2020 and October 2021, 117 nodules in 117 patients with a mass diameter of more than 1 cm were included in the study. Images for measuring the proton density fat fraction (PDFF) and R2 * values were obtained using the iterative decomposition of water and fat with echo asymmetry and least-squares estimation-quantitative technique for liver imaging. Two radiologists independently measured PDFF (%) and R2 * (Hz). Inter-reader agreement and the differences between readers were examined using intra-class correlation coefficient (ICC) and the Bland-Altman method, respectively. PDFF and R2 * values in differentiating liver masses were examined.

Results: The masses included hepatocellular carcinoma (n = 59), cyst (n = 20), metastasis (n = 14), hemangioma (n = 8), and others (n = 16). The ICCs for the region of interest (mm^2), PDFF, and R2 * were 0.988 (95 % confidence interval (CI): 0.983, 0.992), 0.964 (95 % CI: 0.949, 0.975), and 0.962 (95 % CI: 0.941, 0.975), respectively. The differences of measurements between the readers showed that 5.1 % (6/117) and 6.0% (7/117) for PDFF and R2 * , respectively, were outside the 95 % CI.

Conclusion: Our observation indicates that the 6-point Dixon method is applicable to liver masses.

Abbreviations: MRI, magnetic resonance imaging; PDFF, proton density fat fraction; IDEAL-IQ, iterative decomposition of water and fat with echo asymmetry and least-squares estimation-quantitative; ICC, intra-class correlation coefficient; HCC, hepatocellular carcinoma; CI, confidence interval; IP, in-phase; TR, repetition time; TE, echo time; FOV, field of view; HCA, hepatocellular adenoma.

* Corresponding author.
E-mail address: k-kozaka@staff.kanazawa-u.ac.jp (K. Kozaka).

https://doi.org/10.1016/j.ejro.2023.100519
Received 22 June 2023; Received in revised form 10 August 2023; Accepted 16 August 2023
Available online 17 August 2023

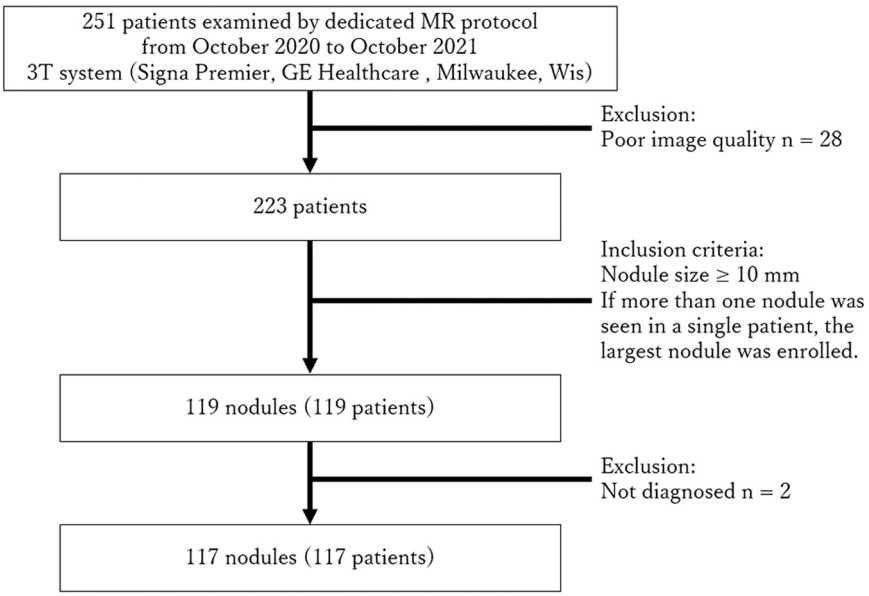

Fig. 1. Flowchart of patient inclusion and exclusion.

Table 1
Summary of the masses.

Mass	n	Mass diametermean [range] (mm)	Chemo-therapy	Basis of diagnosisPathology / Clinical
HCC*	59	27.7 [10.0, 145.2]	6 (10.2 %)	13/46
Cyst	20	29.5 [10.3, 87.2]		1/19
Metastasis†	14	27.0 [12.7, 85.6]	8 (57.1 %)	4/10
Hemangioma	8	34.9 [11.8, 133.4]		0/8
Benign hyperplastic/ regenerative nodule	6	27.5 [16.9, 51.5]		2/4
Inflammatory pseudotumor	4	11.5 [10.5, 11.9]		1/3
Intrahepatic cholangiocarcinoma	3	44.1 [17.5, 72.7]	2 (66.7 %)	3/0
Lymphoma	2	44.0 [36.4, 51.5]		0/2
HCA‡	1	10.6 [10.6, 10.6]		1/0

†: Among the primary malignancy were colon cancer (n = 6), breast cancer (n = 2), pancreatic cancer (n = 2), lung cancer (n = 1), stomach cancer (n = 1), bladder cancer (n = 1), and prostate cancer (n = 1).
‡: It was pathologically diagnosed as inflammatory subtype of hepatocellular adenoma (HCA).
* All hepatocellular carcinoma (HCC) cases in this study had trabecular patterns and were well-differentiated to moderately differentiated HCCs, with some partially accompanying pseudoglandular formation. The subtypes presented in WHO 2019 [29] such as clear cell subtype, macrotrabecular massive, steatohepatitic, scirrhous subtype, etc. were not included.

1. Introduction

Chemical shift magnetic resonance imaging (MRI) techniques have been used for many years to evaluate fat quantification within a specified area [1,2]. Initial practice used the dual-echo technique [1]. However, it is hampered by T1 and T2 * relaxation times which may underestimate fat fraction, especially when T2 * is short, such as in the setting of iron-containing lesions. Several strategies to correct T2 * effects have been evaluated. A breath-hold triple-echo technique has been developed, which consists of a triple-echo spoiled gradient-echo sequence with consecutive first in-phase (IP), opposed-phase, and second IP echo times [3,4]. This method enables the quantification of fat fraction by correcting for T2 * decay and minimizing T1-related effects by using lower flip angle. Moreover, the recent advances in technologies in pulse sequence and reconstruction have made it possible to perform a breath-hold 6-echoe acquisition, so-called a 6-point Dixon method. The 6-point Dixon method offers an accurate way to measure both the fat component and the iron content in the liver, the latter is estimated by T2 * decay. Iterative decomposition of water and fat with echo asymmetry and least-squares estimation-quantitative (IDEAL-IQ), a vendor-provided method, uses this 6-point Dixon approach. It measures proton density fat fraction (PDFF) and R2 * values by modeling multiple fat peaks. Additionally, it corrects for T1 bias, eddy currents, noise bias, and T2 * effects [5–8]. Studies have shown a correlation between the count of steatotic hepatocytes from biopsies and PDFF values. Similarly, a relationship was observed between hepatic iron content and R2 * values. These findings affirm the effectiveness of the 6-point Dixon method in assessing diffuse liver disease [5,6,9–14].

Although the 6-point Dixon method is widely used to quantify fat and iron in diffuse liver disease, its use in evaluating liver masses has been limited. The amount of fat in a hepatic mass is helpful for differential diagnosis and for assessing treatment effect [15,16]. Various amounts of intralesional fat have been reported in hepatocellular carcinoma (HCC), with triple-echo technique reporting a mean fat fraction of 5.7% [3]. Intralesional fat is more common in HCC in its early stage and thus more frequent in well differentiated HCC than in moderately differentiated HCC [17]. Less commonly intralesional fat can be seen in poorly differentiated HCC [18]. Intralesional fat is exceptional in non-HCC malignancy, whereas it is a common in HCC, although not necessarily. Thus, the detection of intralesional fat can help distinguish HCC from other malignant and nonmalignant liver masses. In addition, it has recently been reported that HCC in the setting of non-alcoholic steatohepatitis is more frequently associated with mixed fatty deposits, establishing the steatohepatitic subtype [19,20]. It is known that diffuse fatty deposits also are present in the clear cell subtype of HCC [21]. On the other hand, R2 * value is considered to have a linear correlation with

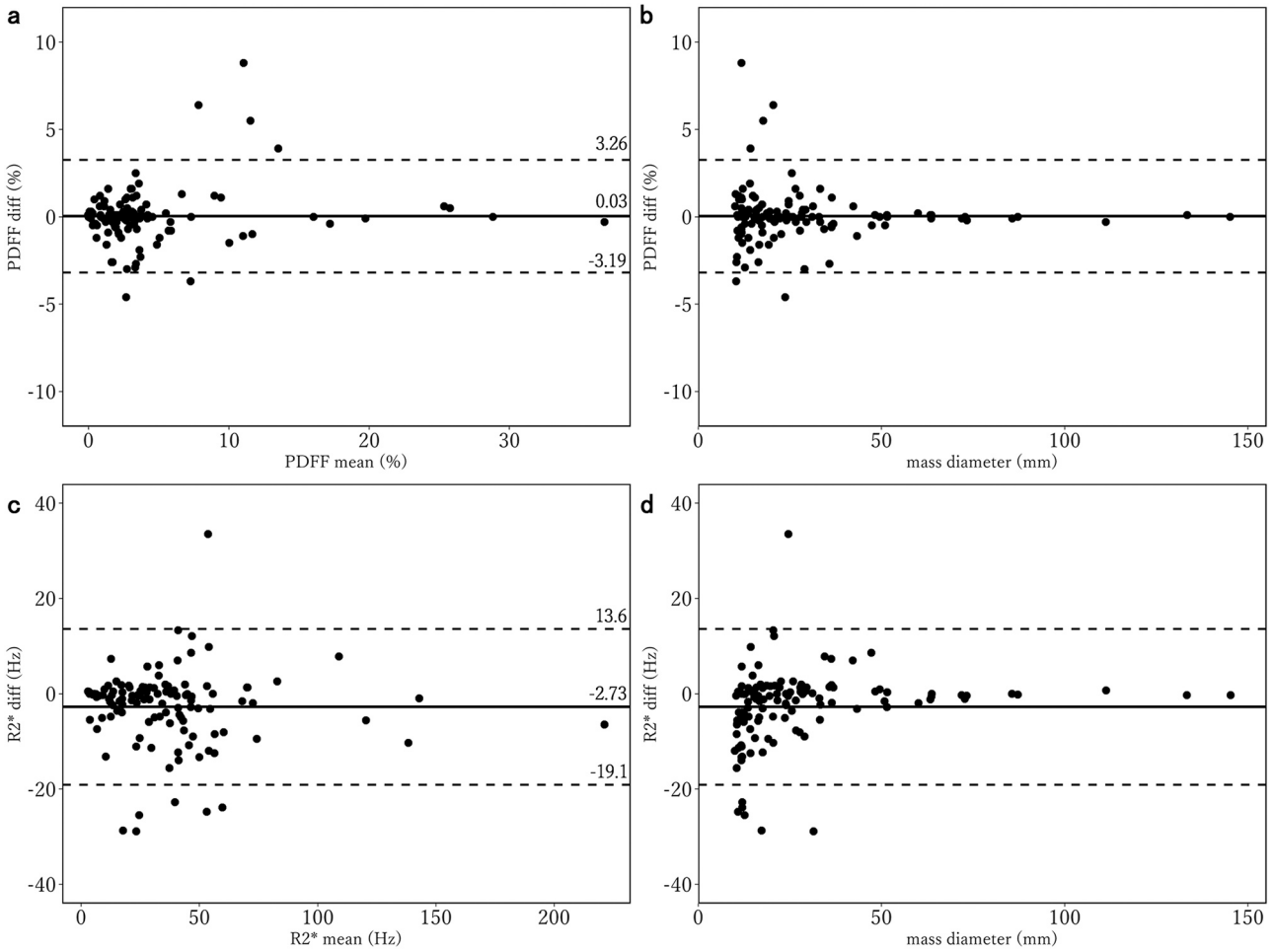

Fig. 2. Scatter plots of proton density fat fraction (PDFF) and R2 * values by the two readers. The vertical line shows the absolute difference between the two measurements and the horizontal one shows either the mean of the two measurements or the mass diameter. PDFF (a, b): There was no proportional bias or fixed bias in PDFF. Most of the subjects were inside the 95% confidence interval (CI); however, six (5.1%) of 117 cases had PDFF values outside the 95% CI (a). Regarding the relationship between PDFF differences and mass diameters, the largest diameter of the outliers was 23.6 mm (b). R2 * (c, d): There was no proportional bias or fixed bias in R2 *. Most of the subjects were inside the 95% CI. However, seven (6.0%) of 117 cases had R2 * values outside the 95% CI (c). Regarding the relationship between R2 * differences and mass diameters, the largest diameter of the outliers was 31.4 mm (d).

liver iron concentration [22], and sensitive to tissue iron deposition secondary to hemorrhagic changes [23]. Its clinical usefulness for hepatic tumors has not yet been clarified. Taken together, assessment of both values of PDFF and R2 * may provide additional quantitative value for characterizing liver masses. However, there is no report to date of utilizing the multi-point Dixon method on liver masses.

The aim of this study was to assess the feasibility of the 6-point Dixon method for evaluating liver masses. We also provide our initial experience with the quantitative values obtained with IDEAL-IQ in various liver masses on a 3 T system.

2. Materials and methods

2.1. Subjects

Our institutional review board approved this retrospective study and waived the requirement for informed patient consent. A board-certificated radiologist (T. M. with 15 years' experience in abdominal radiology) reviewed a database of patients (n = 251) who were more than 18 years old and underwent the 6-point Dixon method in abdominal MRI scans between October 2020 and October 2021, rating the image quality with 3-point scale; as 1) good, image quality with no or minimal image deterioration; 2) intermediate; or 3) poor image quality with extensive respiratory motion artifacts or severe image deterioration and images were not acceptable for evaluating value. Only cases with good image quality were selected and the same reviewer identified patients who had at least one liver mass. Patients with a liver mass less than 1 cm in diameter were excluded because precise quantification of intralesional fat and iron in small masses is difficult. When a patient had multiple liver masses larger than 1 cm, the largest one was selected for evaluation. Two patients were excluded because the diagnosis had not been confirmed. Patients receiving locoregional therapy were excluded, but not those receiving systemic chemotherapy. Ultimately, 117 patients (73 men, 44 women; median age, 67 years; age range, 29–85 years) with 117 nodules were selected for analysis (Fig. 1).

Twenty-five masses (21 %) were diagnosed histologically from biopsy or resection. The remaining 92 masses (79 %) were diagnosed by MRI findings in conjunction with clinical history and follow-up MRI by a board-certificated radiologist (K. K. with 21 years' experience in abdominal radiology). In brief, HCCs were diagnosed when the masses exhibited arterial hyperenhancement and venous or delayed phase washout in high-risk patients, according to the criteria proposed by the Liver Imaging Reporting and Data System v2018. Metastases were diagnosed when the masses demonstrated peripheral rim enhancement and a targetoid appearance (in either or both T2-weighted and diffusion-weighted images) in patients with a known primary malignancy. Cysts were diagnosed when the masses exhibited bright signal intensity on T2-weighted images and no contrast enhancement. Hemangiomas were

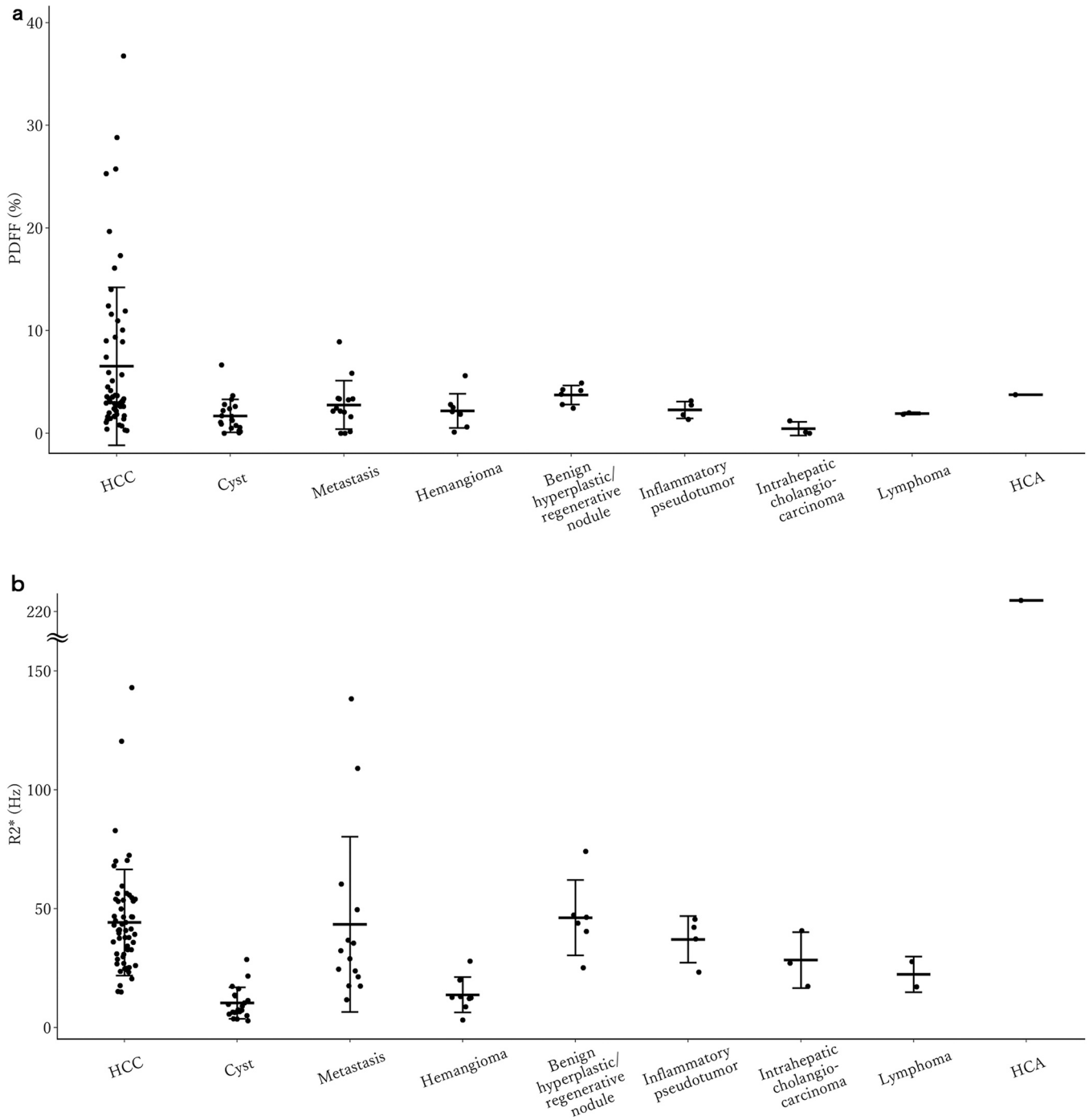

Fig. 3. Scatter plot of proton density fat fraction (PDFF) and R2 * values for each liver mass. Center and error bars indicate mean values and standard deviations for each mass, respectively. a: The mean PDFF values in hepatocellular carcinoma (HCC) were relatively high and dispersed compared to other types of masses. b: The mean R2 * values in cysts and hemangiomas were consistently low compared to other types of masses. HCA: hepatocellular adenoma.

diagnosed when the masses exhibiting high signal intensity on T2-weighted images and a typical dynamic enhancement pattern without interval change. Benign hyperplastic/regenerative nodules were diagnosed when the masses exhibited hyperenhancement in arterial or portal venous phase, the uptake of contrast agent on hepatobiliary phase images, and no or slightly growth of mass size during serial imaging follow-up. Lymphomas were diagnosed when primary and liver masses reduced by underwent chemotherapy in patients with a known lymphoma. Inflammatory pseudotumors were diagnosed when the liver masses reduced rapidly during serial imaging follow-up.

2.2. Image techniques

MR examinations were performed in our institution with an AIR coil at a 3.0 T magnet (Signa Premier, GE Healthcare, Milwaukee, Wis). In addition to our institute standard liver protocol including T2-weigthed images (fat-suppressed fast spin-echo; repetition time (TR)/echo time (TE), 2000–15,000/80–90 msec; flip angle, 90°; field of view (FOV), 40 × 40 cm; matrix, 320 × 224; slice thickness, 4.0 mm), diffusion weighted images (TR/TE, 7500–12,000/64–73 msec; flip angle, 90°; FOV, 40 × 40 cm; matrix, 128 × 160; slice thickness, 6.0 mm; b value, 800 s/mm^2) and fat-suppressed 3D SPGR T1-weighted sequence (TR/

Table 2
Summary of proton density fat fraction (PDFF) and R2 * values for each liver mass.

Mass	n	PDFF mean ± SD [range] (%)	R2* mean ± SD [range] (Hz)
HCC	59	6.52 ± 7.69[0.25, 36.75]	44.2 ± 22.3[15,143]
Cyst	20	1.69 ± 1.60[0, 6.65]	10.3 ± 6.62[2.85, 28.65]
Metastasis	14	2.76 ± 2.38[0, 8.9]	43.4 ± 36.9[11.75, 138.35]
Hemangioma	8	2.18 ± 1.66[0.1, 5.6]	13.8 ± 7.57[3.2, 27.95]
Benign hyperplastic/ regenerative nodule	6	3.72 ± 0.93[2.45, 4.9]	46.2 ± 15.9[25.2, 74.15]
Inflammatory pseudotumor	4	2.26 ± 0.83[1.35, 3.15]	37.1 ± 9.79[23.35, 45.6]
Intrahepatic cholangiocarcinoma	3	0.43 ± 0.67[0, 1.2]	28.4 ± 11.8[17.35, 40.8]
Lymphoma	2	1.93 ± 0.11[1.85, 2]	22.4 ± 7.50[17.1, 27.7]
HCA	1	3.75	221.3

SD: standard deviation
HCC: hepatocellular carcinoma
HCA: hepatocellular adenoma

TE, 3.2–4.0 msec/1.6–2.3 msec; flip angle, 10–15°; FOV, 33–42 cm; matrix, 192 × 320; slice thickness, 4.2 mm) with/without contrast media, a 6-point Dixon sequence (IDEAL-IQ) was performed.

A 6-point Dixon sequence (IDEAL-IQ) had the following parameters: TR, 6.6 msec; TE, six echoes ranging from 0.89 msec to 4.45 msec; FOV, 40 × 32 cm; matrix, 160 × 160; slice thickness, 4.2–10 mm; acquisition time, 18 s (single breath-hold); flip angle, 3°; number of excitations, 0.50; bandwidth, 111.11 kHz; and acceleration factor, Phase 2 × Slice 1.4. PDFF, R2 * map, in phase, opposed phase, water image and fat image were obtained.

2.3. Image evaluations

Images were analyzed using a commercial viewer software package (EV Insite; PSP corporation, Tokyo, Japan) by two radiologists (T. K. with 5 years, and K. K. with 21 years of experience in abdominal radiology) who were blinded to the diagnosis of the liver masses. The readers reviewed all MR images and recorded whether the mass was visible on images obtained with the IDEAL-IQ sequence. A circular region of interest (ROI) was then placed on each visible mass. The size of the ROI was maximized based on the size of each mass. If the mass was not completely visible on any of the images derived from the IDEAL-IQ sequence, we initially recognized the ROI on T2-weighted images. We then used the superimpose (copy and paste) function of the viewer software to transfer this ROI to both the PDFF and R2 * map images for further analysis.

The averaged PDFF and R2 * values of the two readers were used as the representative values of each mass unless the difference between these values was outside the 95% confidence interval (CI). If the values were outside the 95 % CI, the readers assessed the factors that contributed to the differences. Revised ROIs were then placed by consensus of the two readers, and the PDFF and R2 * values thus obtained were submitted as representative of the masses.

2.4. Statistical analysis

Statistical analysis was performed using a graphic user interface for R software (version 3.5.1: the R Foundation for Statistical Computing). Interobserver agreement for the PDFF and R2 * values was assessed by using the intra-class correlation coefficient (ICC), which was illustrated with Bland-Altman plots of the 95% limits of agreement and the absolute difference between the two measurements. P values were computed for each statistic when appropriate. P values < 0.05 were considered to indicate statistical significance.

3. Results

3.1. Characteristics of target masses

A total of 117 masses in 117 patients were evaluated in this study. The mean diameter and standard deviation of the 117 masses were 28.3 ± 23.7 mm. The diagnosis, size, use of chemotherapy, and basis for diagnosis of the liver masses are shown in Table 1.

3.2. Analysis of the interobserver agreement between two readers

Both readers completely identified 71.8 % (84/117) of the masses (completely visible) on at least one image obtained with IDEAL-IQ. The remaining 33 masses were not identified by one or both readers on the images obtained with IDEAL-IQ.

The ICC of ROI area (mm^2), PDFF, and R2 * values for the readers were: 0.988 (95 % CI: 0.983, 0.992), 0.964 (95 % CI: 0.949, 0.975), and 0.962 (95 % CI: 0.941, 0.975), respectively. The differences between the two readers in the PDFF and R2 * values for each liver mass are shown in Fig. 2. There was no proportional bias or fixed bias in each Bland-Altman plot for the two parameters. The values obtained for most of the masses in this study were inside the 95 % CI; however, the PDFF and R2 * values obtained for six (5.1 %) and seven (6.0 %) masses, respectively were outside the 95 % CI. There was no mass for which both the differences in PDFF and R2 * values were outliers.

The reasons for the PDFF outlier cases were masses too small to identify in three cases (10.4 mm, 11.8 mm, and 14.3 mm) and heterogeneous intralesional fat in three cases. As for the 7 masses with outliers in R2*, all of these masses could not be identified on the IDEAL-IQ images and four of them were small (10.9 mm, 11.9 mm, 12.1 mm, and 12.7 mm). There were no statistical differences between the readers in PDFF and R2 * values for all masses ($n = 117$). However, when comparing only the PDFF and R2 * values between the readers for the masses not visible on the IDEAL-IQ images ($n = 33$), there were significant differences for both PDFF and R2 * ($p < 0.01$).

3.3. Quantitative analysis of the PDFF and R2 * values of the liver masses

Fig. 3 shows scatter plots of the PDFF and R2 * values for each mass, and the values (means and standard deviation) of each group are shown in Table 2. Fig. 4 shows representative tumors. The mean PDFF of the masses were 6.52% (95% CI: 4.52, 8.52) for HCC, 1.69% (95% CI: 0.93, 2.44) for cysts, 2.76% (95% CI: 1.40, 4.12) for metastases, 2.18% (95% CI: 0.79, 3.58) for hemangiomas, 3.72% (95% CI: 2.75, 4.70) for benign hyperplastic/regenerative nodules, 2.26% (95% CI: 0.93, 3.60) for inflammatory pseudotumors, 0.43% (95% CI: −1.20, 2.07) for intrahepatic cholangiocarcinomas, 1.93% (95% CI: 1.04, 2.81) for lymphomas, and 3.75% for hepatocellular adenoma (HCA). The R2 * values were 44.2 Hz (95% CI: 38.4, 50.0) for HCC, 10.3 Hz (95%

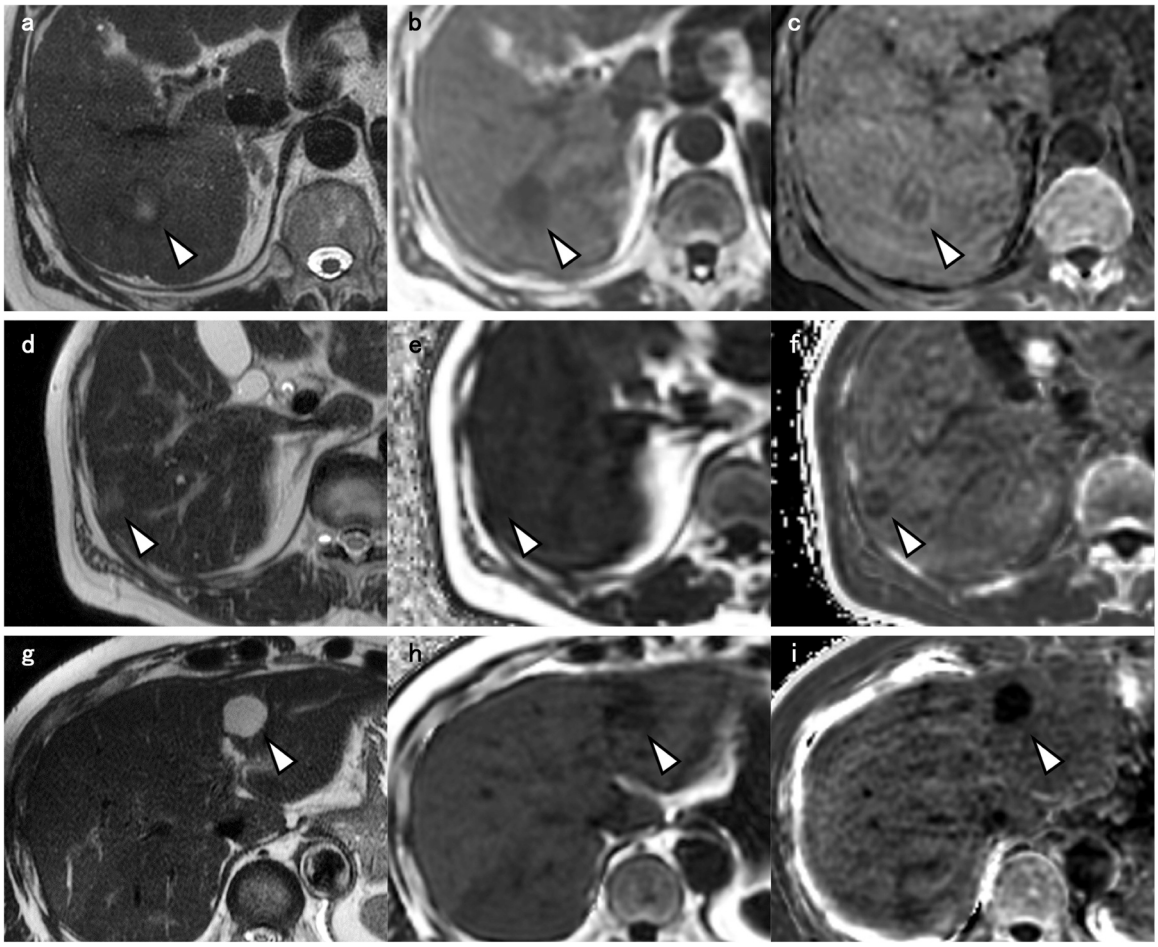

Fig. 4. Representative cases. a-c: A case of therapeutic naïve hepatocellular carcinoma in a 59-year-old man with steatosis. T2-weighted MR image shows heterogenous signal intensity mass in the posterior segment of the right liver lobe (a: arrowhead). The mass is visible both on proton density fat fraction (PDFF) and R2 * maps (b, c: arrowhead). PDFF and R2 * values are 19.7% and 70.4 Hz, respectively. d-f: A case of focal nodular hyperplasia (categorized into benign hyperplastic/ regenerative nodules in this study) in a 64-year-old woman. T2-weighted MR image shows moderate-to-high signal intensity mass in the posterior segment of the right liver lobe (d: arrowhead). The mass is visible on R2 * map, but not on PDFF (e, f: arrowhead). PDFF and R2 * values are 4.15% and 44.0 Hz, respectively. g-i: A case of hemangioma in a 43-year-old man. T2-weighted MR image shows high signal intensity mass in the lateral section of the liver (g: arrowhead). The mass is visible on both PDFF and R2 * maps (h, i: arrowhead). PDFF and R2 * values are 2.1% and 3.2 Hz, respectively.

CI: 7.23, 13.4) for cysts, 43.4 Hz (95% CI: 22.1, 64.7) for metastases, 13.8 Hz (95% CI: 7.61, 20.0) for hemangiomas, 46.2 Hz (95% CI: 29.6, 62.9) for benign hyperplastic/regenerative nodules, 37.1 Hz (95% CI: 21.6, 52.7) for inflammatory pseudotumors, 28.4 Hz (95% CI: −0.84, 57.7) for intrahepatic cholangiocarcinomas, 22.4 Hz (95% CI: −44.9, 89.7) for lymphomas, and 221.3 Hz for HCA.

The mean PDFF of HCC was higher and more variable than that of other masses in this study. The mean R2 * values of cysts and hemangiomas were consistently low. No significant difference was observed with or without chemotherapy in both HCC and metastases (Fig. 5).

4. Discussion

In this study, we measured PDFF and R2 * values of various liver masses and examined their characteristics. The agreement rate of measurement between two observers was excellent for liver masses larger than 1 cm, and the PDFF and R2 * values appeared to reflect the characteristics of the various masses studied, suggesting that fat and iron quantification of liver masses may be one of useful values for differential diagnosis.

In our efforts to achieve a high degree of agreement between the two readers, we implemented a number of strategies that we believe led to obtaining reliable quantitative values for liver masses. These strategies included the following: (i) we focused on nodules that were 1 cm or larger, thereby limiting the influence of size-related challenges often associated with smaller nodules, such as their visibility and the impact of minor artifacts; (ii) including cases with good image quality allowed us to maintain a high standard of image clarity and resolution, thereby enhancing the reliability of our measurements; and (iii) utilizing the superimpose (copy and paste) function. This technique provided us with a consistent and replicable approach to measuring liver masses, thus increasing the reliability and consistency of our findings. The Bland-Altman method, which can analyze the differences of measurements between the readers, showed that 5.1% (6/117) and 6.0% (7/117) of measurements of PDFF and R2 * , respectively, were outside the 95% CI. The possible causes for these differences were as follows; (i) the small size of the masses, (ii) the invisibility of the masses, or (iii) minute artifacts. In fact, smaller masses tended to show larger differences in both PDFF and R2 * values. Although our study focused solely on cases with good image quality, smaller masses were often less clearly visualized. Minor noise and motion-related artifacts, which were not visually detectable, might become more pronounced, especially in these smaller masses. The multi-point Dixon method is sensitive to body motion, and local artifacts may limit the reliability of the values [24]. In our study, 28 out of 251 (11.2%) cases were excluded during case selection due to poor image quality. The causes of image quality degradation included

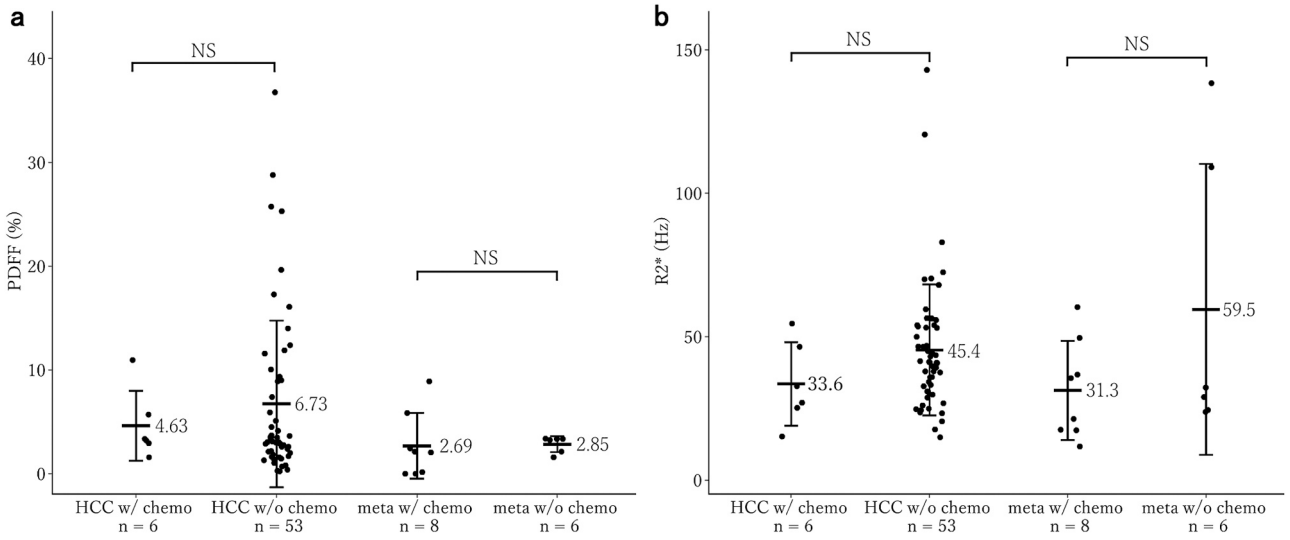

Fig. 5. Scatter plot of proton density fat fraction (PDFF) and R2 * values with and without chemotherapy in hepatocellular carcinoma (HCC) and metastasis. a: The mean PDFF of masses was 4.63% for HCC with chemotherapy (n = 6), 6.73% for HCC without chemotherapy (n = 53), 2.69% for metastasis with chemotherapy (n = 8) and 2.85% for metastasis without chemotherapy (n = 6). No significant difference was observed with or without chemotherapy in both HCC and metastases. b: The mean R2 * of masses was 33.6 Hz for HCC with chemotherapy (n = 6), 45.4 Hz for HCC without chemotherapy (n = 53), 31.3 Hz for metastasis with chemotherapy (n = 8) and 59.5 Hz for metastasis without chemotherapy (n = 6). No significant difference was observed with or without chemotherapy in both HCC and metastases.

poor breath-holding and inability to evaluate peripheral liver masses due to artifacts from cardiac pulsation or intestinal peristalsis, especially in the case of small masses. To overcome these problems, especially when evaluating small liver masses, it is necessary to set up a protocol that reduces image acquisition time by adjusting slice thickness and in-plane spatial resolution, in addition to setting an appropriate reduction factor of parallel imaging.

This study serves as an initial exploratory assessment, encompassing a wide variety of mass types. We acknowledge that, in certain instances, the limited sample size may preclude definitive conclusions. Nonetheless, we posit that the dissemination of our quantified results holds potential value for informing future research endeavors and advancing clinical applications. In the present study, the mean PDFF of HCC was relatively high (6.52 [range: 0, 36.5]), whereas the mean PDFF of other masses ranged from 0.43 to 3.72. Several liver masses including HCC, HCA, and hepatic angiomyolipoma may contain fat [15]. In HCC, intralesional fat is more frequently observed in well-differentiated HCCs [25], although intralesional fat is reported to occur even in poorly-differentiated HCC [18]. Furthermore, a subtype of HCC, steatohepatitic HCC, characterized by fibrosis, inflammation and intralesional fat in the mass, has more recently been identified [19,20]. Thus, the use of PDFF has the potential to contribute not only to the diagnosis of liver masses but also to the diagnosis of HCC subtypes. Interestingly, in this study one colorectal liver metastasis after chemotherapy had a PDFF above 6.5% (a proposed cutoff value of PDFF for fatty liver [11]). Intratumoral lipid either in areas of necrosis or as cytoplasmic lipid droplets has been reported in malignant tumors after chemotherapy [26]. In addition, Nakai, et al. reported that intralesional fat in colorectal liver metastases treated with preoperative chemotherapy could be identified in dual-echo gradient-recalled echo MR images [16]. Thus, PDFF could be a biomarker of treatment response in liver metastases.

R2 * is a parameter that reflects heterogeneity of the magnetic field in tissue [6]. It has a high value when there is more iron deposition in the tissue. In this study, R2 * values were low for liver cysts and hemangiomas but varied widely for other masses. The variability was particularly high in HCC and liver metastases, which often cause hemorrhagic necrosis. Moreover, hemorrhagic necrosis in HCCs has been reported to occur after administration of molecular-targeted drugs such as sorafenib [27], whereas it generally does not occur after conventional chemotherapy or radiotherapy. Our patient cohort included very few patients treated with molecular-targeted therapy (n = 6). Because of that, in this study, there were no significant differences in R2 * between HCC with or without chemotherapy. Whether the value of R2 * in the mass is a promising imaging marker of therapeutic efficacy is inconclusive in this study and further studies are needed to clarify this issue. The variability was relatively small for lymphoma and intrahepatic cholangiocarcinoma. This result seems reasonable as intratumor degeneration is presumed to be relatively low in lymphomas. However, only two lymphomas were included in this study. Conversely, our single HCA case exhibited a high R2 * value, potentially indicative of iron deposition as suggested in previous reports. Nevertheless, given the limited sample size, further investigation is required for confirmation [28].

This study had several limitations. First, selection bias is inevitable because of the retrospective design. Second, the number of cases is relatively small. This study was a preliminarily study to evaluate the usefulness of IDEAL-IQ for characterizing liver masses. Further study is needed to clarify the significance of PDFF and R2 * of liver masses. Third, radiologic-pathologic correlation could not be performed because of the lack of pathologic specimens for the majority of masses. It would be interesting to see what histological background the R2 * value reflects. Finally, slice thickness of IDEAL-IQ imaging was not consistent. However, slice thickness was less than 10 mm in all cases, which likely had a minimal impact on this study which included only nodules larger than 1 cm.

5. Conclusion

PDFF and R2 * values of liver masses imaged on a 3 T MRI system can be obtained with excellent concordance between two readers. Our observation indicates that the 6-point Dixon method is applicable to liver masses and might yield quantitative values useful for characterizing them. Further case accumulation is needed to establish the utility of PDFF and R2 * as new quantitative markers of liver masses.

Ethical approval

The Institutional Review Board of Kanazawa University Graduate

School of Medical Sciences approved this retrospective study (2016–181), and informed consent was waived.

1)The scientific guarantor of this publication is Kazuto Kozaka, M.D., Ph.D.

2)The authors of this manuscript declare no relationships with any companies, whose products or services may be related to the subject matter of the article.

3)This study doesn't receive funding.

4)No complex statistical methods were necessary for this paper.

5)Only if the study is on human subjects: Written informed consent was waived by the Institutional Review Board.

6)Methodology:

- retrospective
- observational
- performed at one institution

Informed consent and ethical statement

This is an institutional review board approved, HIPPA-compliant retrospective study, and the need to obtain informed consent was waived.

Funding

- This study has not received any funding.
- The authors state that this work has not received any funding.

CRediT authorship contribution statement

Taichi Kitagawa: Data curation, Formal analysis, Investigation, Visualization, Writing – original draft, Writing – review & editing. **Kazuto Kozaka**: Conceptualization, Data curation, Formal analysis, Investigation, Methodology, Project administration, Supervision, Validation, Visualization, Writing – original draft, Writing – review & editing. **Takashi Matsubara**: Data curation, Writing – review & editing. **Tetsuya Wakayama**; Writing – review & editing. **Atsushi Takamatsu**: Software, Writing – review & editing. **Tomohiro Kobayashi**: Formal analysis, Writing – review & editing. **Kenichiro Okumura**: Formal analysis, Writing – review & editing. **Kotaro Yoshida**: Data curation, Writing – review & editing. **Norihide Yoneda**: Conceptualization, Writing – review & editing. **Azusa Kitao**: Conceptualization, Data curation, Writing – review & editing. **Satoshi Kobayashi**: Supervision, Validation, Writing – review & editing. **Toshifumi Gabata**: Resources, Writing – review & editing. **Osamu Matsui**: Supervision, Writing – review & editing. **Jay P Heiken**: Writing – review & editing.

Declaration of Competing Interest

The authors declare that they have no known competing financial interests or personal relationships that could have appeared to influence the work reported in this paper.

Acknowledgments

We thank Mr. Richard Curtis for manuscript proofreading.

References

[1] W.T. Dixon, Simple proton spectroscopic imaging, Radiology 153 (1) (1984) 189–194, https://doi.org/10.1148/radiology.153.1.6089263.
[2] S.B. Reeder, I. Cruite, G. Hamilton, C.B. Sirlin, Quantitative assessment of liver fat with magnetic resonance imaging and spectroscopy, J. Magn. Reson Imaging 34 (4) (2011) 729–749, https://doi.org/10.1002/jmri.22775.
[3] S. Nougaret, B. Monsonis, N. Molinari, et al., Quantification of liver fat content in liver and primary liver lesions using triple-echo-gradient-echo MRI, Eur. Radio. 30 (9) (2020) 4752–4761, https://doi.org/10.1007/s00330-020-06757-1.
[4] J. Satkunasingham, C. Besa, O. Bane, et al., Liver fat quantification: comparison of dual-echo and triple-echo chemical shift MRI to MR spectroscopy, Eur. J. Radio. 84 (8) (2015) 1452–1458, https://doi.org/10.1016/j.ejrad.2015.05.001.
[5] S. Eskreis-Winkler, G. Corrias, S. Monti, et al., IDEAL-IQ in an oncologic population: meeting the challenge of concomitant liver fat and liver iron, Cancer Imaging 18 (1) (2018), https://doi.org/10.1186/s40644-018-0167-3.
[6] K. Imajo, T. Kessoku, Y. Honda, et al., MRI-based quantitative R2(*) mapping at 3 Tesla reflects hepatic iron overload and pathogenesis in nonalcoholic fatty liver disease patients, J. Magn. Reson Imaging 55 (1) (2022) 111–125, https://doi.org/10.1002/jmri.27810.
[7] S.D. Serai, J.R. Dillman, A.T. Trout, Proton density fat fraction measurements at 1.5- and 3-T hepatic MR imaging: same-day agreement among readers and across two imager manufacturers, Radiology 284 (1) (2017) 244–254, https://doi.org/10.1148/radiol.2017161786.
[8] C.-Y. Liu, C.A. McKenzie, H. Yu, J.H. Brittain, S.B. Reeder, Fat quantification with IDEAL gradient echo imaging: correction of bias fromT1 and noise, Magn. Reson Med 58 (2) (2007) 354–364, https://doi.org/10.1002/mrm.21301.
[9] P. Bannas, H. Kramer, D. Hernando, et al., Quantitative magnetic resonance imaging of hepatic steatosis: Validation in ex vivo human livers, Hepatology 62 (5) (2015) 1444–1455, https://doi.org/10.1002/hep.28012.
[10] Ilkay S. Idilman, Hatice Aniktar, Ramazan Idilman, et al., Hepatic steatosis: quantification by proton density fat fraction with MR imaging versus liver biopsy, Radiology 267 (3) (2013) 767–775, https://doi.org/10.1148/radiol.13121360.
[11] A. Tang, A. Desai, G. Hamilton, et al., Accuracy of MR imaging-estimated proton density fat fraction for classification of dichotomized histologic steatosis grades in nonalcoholic fatty liver disease, Radiology 274 (2) (2015) 416–425, https://doi.org/10.1148/radiol.14140754.
[12] V. Ajmera, C.C. Park, C. Caussy, et al., Magnetic resonance imaging proton density fat fraction associates with progression of fibrosis in patients with nonalcoholic fatty liver disease, e2, Gastroenterology 155 (2) (2018) 307–310, https://doi.org/10.1053/j.gastro.2018.04.014.
[13] H.H. Hu, T. Yokoo, M.R. Bashir, et al., Linearity and bias of proton density fat fraction as a quantitative imaging biomarker: a multicenter, multiplatform, multivendor phantom study, Radiology 298 (3) (2021) 640–651, https://doi.org/10.1148/radiol.2021202912.
[14] İlkay S. İdilman, Deniz Akata, Mustafa Nasuh Özmen, Mu.şturay Karçaaltıncaba, Different forms of iron accumulation in the liver on MRI, Diagn. Inter. Radio. 22 (1) (2016) 22–28, https://doi.org/10.5152/dir.2015.15094.
[15] S.R. Prasad, H. Wang, H. Rosas, et al., Fat-containing lesions of the liver: radiologic-pathologic correlation, Radiographics 25 (2) (2005) 321–331, https://doi.org/10.1148/rg.252045083.
[16] Y. Nakai, W. Gonoi, A. Hagiwara, et al., MRI detection of intratumoral fat in colorectal liver metastases after preoperative chemotherapy, AJR Am. J. Roentgenol. 210 (5) (2018) W196–W204, https://doi.org/10.2214/AJR.17.18814.
[17] M. Kadoya, O. Matsui, T. Takashima, A. Nonomura, Hepatocellular carcinoma: correlation of MR imaging and histopathologic findings, Radiology 183 (3) (1992) 819–825, https://doi.org/10.1148/radiology.183.3.1316622.
[18] Y. Asayama, A. Nishie, K. Ishigami, et al., Fatty change in moderately and poorly differentiated hepatocellular carcinoma on MRI: a possible mechanism related to decreased arterial flow, Clin. Radio. 71 (12) (2016) 1277–1283, https://doi.org/10.1016/j.crad.2016.04.020.
[19] M. Taniai, E. Hashimoto, M. Tobari, et al., Clinicopathological investigation of steatohepatitic hepatocellular carcinoma: a multicenter study using immunohistochemical analysis of adenoma-related markers, Hepatol. Res. 48 (12) (2018) 947–955, https://doi.org/10.1111/hepr.13203.
[20] M. Salomao, W.M. Yu, R.S. Brown Jr., J.C. Emond, J.H. Lefkowitch, Steatohepatitic hepatocellular carcinoma (SH-HCC): a distinctive histological variant of HCC in hepatitis C virus-related cirrhosis with associated NAFLD/NASH, Am. J. Surg. Pathol. 34 (11) (2010) 1630–1636, https://doi.org/10.1097/PAS.0b013e3181f31caa.
[21] H. Wang, B. Tan, B. Zhao, G. Gong, Z. Xu, CT findings of primary clear cell carcinoma of liver: with analysis of 19 cases and review of the literature, Abdom. Imaging 39 (4) (2014) 736–743, https://doi.org/10.1007/s00261-014-0104-2.
[22] B. Henninger, J. Alustiza, M. Garbowski, Y. Gandon, Practical guide to quantification of hepatic iron with MRI, Eur. Radio. 30 (1) (2020) 383–393, https://doi.org/10.1007/s00330-019-06380-9.
[23] M. Sun, S. Wang, Q. Song, et al., Utility of R2* obtained from T2*-weighted imaging in differentiating hepatocellular carcinomas from cavernous hemangiomas of the liver, PLoS One 9 (3) (2014), e91751, https://doi.org/10.1371/journal.pone.0091751.
[24] U. Motosugi, D. Hernando, P. Bannas, et al., Quantification of liver fat with respiratory-gated quantitative chemical shift encoded MRI, J. Magn. Reson Imaging 42 (5) (2015) 1241–1248, https://doi.org/10.1002/jmri.24896.
[25] R. Kutami, Y. Nakashima, O. Nakashima, K. Shiota, M. Kojiro, Pathomorphologic study on the mechanism of fatty change in small hepatocellular carcinoma of humans, J. Hepatol. 33 (2) (2000) 282–289, https://doi.org/10.1016/s0168-8278(00)80369-4.
[26] X. Pan, M. Wilson, C. McConville, et al., Increased unsaturation of lipids in cytoplasmic lipid droplets in DAOY cancer cells in response to cisplatin treatment, Metabolomics 9 (3) (2013) 722–729, https://doi.org/10.1007/s11306-012-0483-8.
[27] C. Schraml, N.F. Schwenzer, P. Martirosian, et al., Diffusion-weighted MRI of advanced hepatocellular carcinoma during sorafenib treatment: initial results, AJR

Am. J. Roentgenol. 193 (4) (2009) W301–W307, https://doi.org/10.2214/AJR.08.2289.

[28] Sonja Gordic, Swan N. Thung, Sasan Roayaie, Mathilde Wagner, Bachir Taouli, Hepatic adenomatosis in liver cirrhosis, EJR Open (2017) 115–117, https://doi.org/10.1016/j.ejro.2017.08.001.

[29] M. Torbenson, I. Ng, Y. Park, M. Roncalli, M. Sakamoto, Hepatocellular carcinoma. WHO classification of tumours Digestive System Tumours, 5 ed..,, IARC,, Lyon, 2019, pp. 229–239.